The Journal of Experimental Biology 211, 1668-1680
Published by The Company of Biologists 2008
doi:10.1242/jeb.015289

The relationship between shape of the skull and bite force in finches

Maria A. A. van der Meij and Ron G. Bout*

Evolutionary Morphology, Institute of Biology Leiden, Leiden University, Clusius Laboratory/EMCA, Wassenaarseweg 64, PO Box 9505, 2300 RA Leiden, The Netherlands

*Author for correspondence (e-mail: r.g.bout@biology.leidenuniv.nl)

Accepted 11 March 2008

SUMMARY

In finches husking time is non-linearly related to the ratio of seed hardness to maximal bite force. Fringillids produce larger bite force and husk relatively hard seeds faster than estrildids of similar size. This is at least partly explained by their relatively larger jaw muscle mass and a difference in husking technique. However, the effect of differences in skull geometry on bite force is unclear. In this study differences in skull morphology that may contribute to the difference in bite force between fringillids and estrildids are analyzed. The shape of the skull was described by the 3D coordinates of a set of landmarks and, after eliminating size, the effect of differences in the shape of the skull on bite force was determined using a static force model. EMG recordings of jaw muscles during seed cracking were used to validate assumptions about the muscle activation patterns used for the static bite force model. The analysis shows that most of the variation in skull geometry is related to differences in size. Although the shape of the skull is highly convergent between fringillids and estrildids, the shape of the skull differs significantly between the two groups. A principal component analysis of the landmark coordinates shows several patterns of allometric shape changes, one of which is expressed more strongly in estrildids than in fringillids. Three characters dominate the effect of shape changes on bite force. Bite force increases with a more caudal position of the quadrate, a more downward inclined beak and a relatively short jugal and palatine. A more downward inclined beak is typically found in estrildids. The height of the upper bill and a number of other changes in skull shape have little effect on bite force. An estimate of the relative contributions of jaw muscle size and skull geometry to the difference in bite force between fringillids and estrildids suggests that the contribution of muscle size is much larger than the contribution of skull geometry.

Key words: bite force, feeding, finch, morphometrics, skull.

INTRODUCTION

Darwin's finches and Hawaiian honeycreepers provide some of the best known examples of adaptive radiation, both of which are characterised by a large diversity of beak shapes (Raikow, 1977; Grant, 1986). The evolutionary mechanisms underlying the divergence of feeding habits and beak morphology during adaptive radiation have been studied extensively (Grant, 1986; Grant and Grant, 1989). Variation in food availability and interspecific competition result in natural selection for specific feeding habits and beak morphologies in a number of species (Boag and Grant, 1981; Schluter and Smith, 1986; Smith, 1991; Grant and Grant, 1995) and beak size has been identified as the most variable trait in cardueline finches (Björklund, 1991).

While beak size and shape may reflect the hardness and shape of the seeds taken by different species much less is known about the variability of the traits that determine bite force directly. Bite force is influenced by body size, the geometry of the skull and jaw closing muscles, and the relative size of the jaw closing muscles. The variation in beak shape in some groups of finches is in contrast with results from studies on closely related species that show very little variation in beak shape and very large variation in overall size among species (Björklund and Merilä, 1993). The lack of divergence in beak shape in the presence of natural selection is interpreted as shared adaptation to similar feeding modes (Merilä and Björklund, 1999), rather than the presence of long-term developmental constraints (Arnold, 1991).

Most studies on the efficiency of feeding in finches concentrate on husking time in relation to seed size, seed hardness and body size (Kear, 1962; Hespenheide, 1966; Willson, 1971; Schluter, 1982; Smith, 1987; Díaz, 1990; Read, 1991; van der Meij et al., 2004). Although body size may play an important role in establishing differences in husking performance and therefore in occupying different trophic niches (Björklund and Merilä, 1993), taxon-specific differences in seed handling efficiency have been reported. Fringillids and estrildids belong to two separate families (van der Meij et al., 2005) and differ in their ability to crack seeds efficiently. Fringillids crack closed shelled seeds faster than estrildids of the same body size and have relatively larger jaw muscles and a higher maximal bite force (van der Meij and Bout, 2004; van der Meij et al., 2004). Differences in maximal bite force may depend not only on differences in jaw muscle force, but also on differences in the geometry of the cranial elements (skull shape).

In Galápagos finches bite force is not only related to beak size but also to head width (Herrel et al., 2005a; Herrel et al., 2005b). While some differences in skull morphology may be the consequence of a large bite force, e.g. by increasing the attachment area for jaw muscles or by increasing the resistance to reaction forces, other differences may be directly related to an increase in bite force by affecting the lever arms of muscles. A high upper bill (kinetic hinge), for instance, is often interpreted as an adaptation to large bite force because it increases the moment of the upper jaw closing muscles (Bowman, 1961; Bock, 1966). In this study we use the 3D coordinates of a set of landmarks representing the positions of the joints between neurocranium, quadrate, pterygoid, palatine, jugal and upper and lower jaw of the skull of finches to quantify

differences in the shape of the skull between and within two groups of finches: the fringillids and estrildids. A Generalised Procrustes Analysis was used to eliminate differences in size between the skulls.

The effect of differences in the shape of the skull on maximum bite force was determined using a 2D static force model. EMG recordings of jaw muscles during seed cracking were made to check assumptions about the muscle activation patterns used for the static bite force model.

MATERIALS AND METHODS

Species

For the morphometric analysis we used the skulls of 42 taxa: 20 species of the family Fringillidae and 22 species of the family Estrildidae [Table 1; taxonomical names are according to Sibley and Monroe (Sibley and Monroe, 1990; Sibley and Monroe, 1993)]. Most species were purchased commercially and sacrificed with an overdose of the anaesthetic Nembutal (Sanofi Sante B.V., Maassluis, The Netherlands). Frozen specimens (–20°C) from a small number of species were kindly made available to us by the Department of Experimental Zoology of Wageningen University. After removing most of the tissue, the skulls were cleaned with the help of enzyme-enriched washing power (non-alkaline Biotex, at a temperature of 37°C). The lower jaw was removed from the skull to get a better view of the ventral side of the skull.

Table 1. Species used for morphometric analysis

Family, Species	Common names	Body mass (g)
Fringillidae		
Fringilla montifringilla	Brambling	17.1
Fringilla coelebs	Chaffinch	19.9
Carduelis carduelis	European goldfinch	16.8
Carduelis cucullata	Red siskin	10.8
Carduelis chloris	Greenfinch	28.3
Carduelis sinica	Oriental greenfinch	20.0
Rhodopechys obsoleta	Desert finch	22.5
Rhodopechys mongolica	Mongolian trumpeter finch	19.0
Serinus serinus	Serin	11.1
Serinus leucopygius	White-rumped seedeater	9.5
Serinus atrogularis	Yellow-rumped seedeater	10.4
Uragus sibericus	Long-tailed rosefinch	13.0
Carpodacus rubicilloides	Eastern great rosefinch	36.0
Carpodacus roseus	Pallas's rosefinch	21.1
Carpodacus puniceus	Red-breasted rosefinch	16.5
Coccothraustes coccothraustes	Hawfinch	54.4
Mycerobas affinis	Collared grosbeak	70.0
Eophona migratoria	Yellow-billed grosbeak	52.0
Pyrrhula pyrrhula	Eurasian bullfinch	20.8
Pyrrhula leucogenus	Philippine bullfinch	22.9
Estrildidae		
Padda oryzivora	Java sparrow	30.4
Chloebia gouldiae	Gouldian finch	15.2
Erythrura prasina	Pin-tailed parrotfinch	15.4
Taeniopygia bichenovii	Black-throated finch	9.7
Amandava subfava	Zebra waxbill	6.8
Lonchura maja	White-headed munia	13.2
Lonchura fringilloides	Magpie mannikin	16.2
Lonchura caniceps	Grey-banded mannikin	14.4
Lonchura stygia	Black mannikin	11.1
Neochima ruficauda	Star finch	12.1
Neochmia modesta	Plum-headed finch	13.2
Estrilda caerulescens	Lavender waxbill	8.4
Estrilda astrild	Common waxbill	7.5
Pytilia melba	Green-winged pytilia	13.5
Mandingoa nitidula	Green-backed twinspot	13.5
Cryptospiza reichenovii	Red-faced crimson-wing	14.3
Pyrenestes sanguineus	Crimson seedcracker	18.0
Hypargos niveoguttatus	Peters twinspot	15.7
Uraeginthus cyanocephalus	Blue-capped cordon-blue	10.0
Spermophaga haematina	Western bluebill	22.3
Euschistopiza dybowskii	Dybowski's dusky twinspot	11.4
Amadina fasciata	Cut-throat finch	18.5

Landmarks

To analyze the shape of the skull as well as the length of the different skull elements we reconstructed the 3D coordinates of a number of landmarks from a series of images of skulls rotated along their long axis. A digital camera (Nikon Coolpix 950) was set at a fixed distance of 30 cm from the skull. The digital images had a resolution of 1200×1600 and for very small skulls the digital zoom was used (max. 2×). The skulls were clamped at the top of the orbital region and fixed to a rotating device in such a way that the long axis of the skull was in line with the rotation axis of the device (Fig. 1). The rotating device had a wheel with a pin to select fixed rotation intervals. The skull was then rotated along its longitudinal axis and seven digital images were taken at –60°, –30°, 0°, 30°, 60°, 90° and 120° (Fig. 2), where 0° represents a lateral view of the skull and 90° a ventral view of the skull. Two metal *XYZ* frames, one fixed to the stationary part of the rotating device and one fixed to the rotation axis of the device, were used to check for unintended translations or rotation of the skull with respect to the camera. For each skull a selected set of natural landmarks (e.g. joints, the tip of processi; see Table 2) were digitised. If necessary the position of less well-defined landmarks was marked on the skull with ink (e.g. the base of processus postorbitalis) to assure that the same point was measured in all images. A piece of millimetre-marked paper was used to calculate the scaling factor for the images.

Custom made software written in MatLab 5.3 (The Mathworks Inc, Natick, MA, USA) was used to reconstruct the 3D coordinates of the landmarks. For each point a first estimate of its unknown third coordinate was chosen. A search matrix was created by adding a random component to a series of 10 values of the first estimate for each individual measurement. The series of photographs containing the landmark were then all rotated to the same orientation

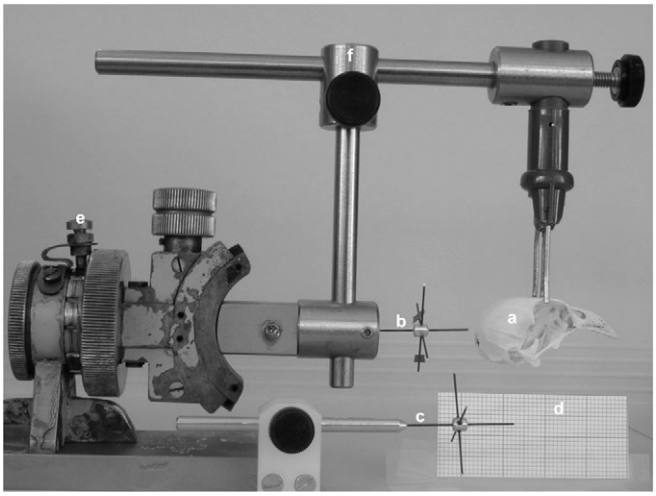

Fig. 1. Rotating device used to take photographs of a rotating skull. A, skull; b, fixed *XYZ* axes; c, rotating *XYZ* axes; d, millimeter paper; e, pin to set the angle; f, adjustable tubes.

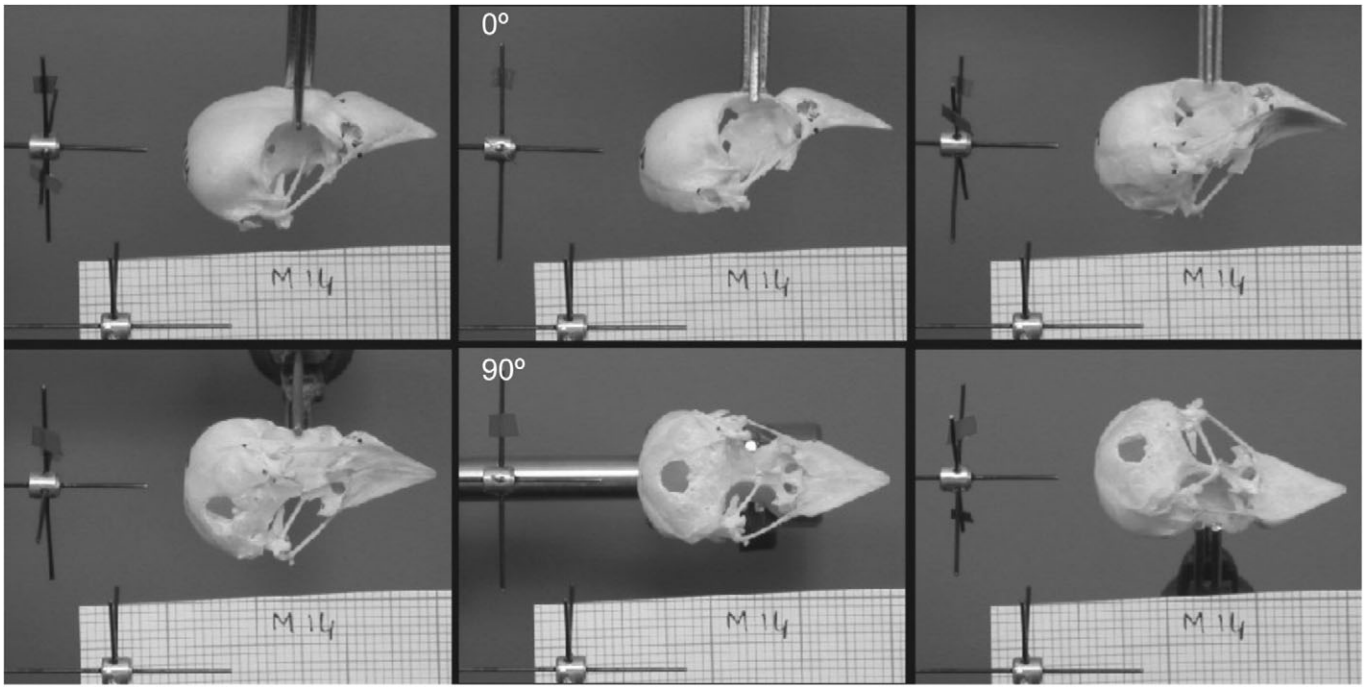

Fig. 2. An example of a series of images taken from a skull (6 out of 7 shown), The skull was rotated along its longitudinal axis with an interval of 30°; 0° represents a lateral view of the skull and 90° a ventral view of the skull.

(0°) after a correction for the projection angle. The combined standard deviation (s.d.) over all x, y and z measurements in the 0° rotation plane was used as a cost function that was minimized with a steepest gradient descent method [Nelder and Mead simplex method (Bunday, 1984)] by adjusting the z-value. This effectively gave the same results as starting with random y and z-values in the 0° rotation plane (x does not change under the rotation scheme used) and minimizing the difference with the measured x,y values after rotation of the initial coordinates towards the plane in which they were measured.

Table 2. Landmarks of the skull

Left, right	Landmark
1	Most rostral point orbita
2	Most caudal point orbita
3	Middle of frontonasal hinge
4	Tip upper beak
5	Most lateral connection between quadrate and skull (capitulum otic quadrati)
6	Most medial connection between quadrate and mandible (condylus medialis quadrati)
7	Most lateral connection between quadrate and mandible (condylus lateralis quadrati)
8	Most caudal connection between quadrate and mandible (condylus caudalis quadrati)
9	Tip processus orbitalis quadratum
10	Connection jugal–quadrate
11, 12c	Connection quadrate–pterygoid
13	Connection palatine–pterygoid
14, 15c	Tip processus transpalatinus
16, 17c	Angulus caudolateralis of palatine
18, 19c	Connection palatine–upper beak
20	Lateral position of connection jugal–upper beak
21, 22c	Ventral position of connection jugal–upper beak
23	Base processus postorbitalis
24	Tip processus postorbitalis
25	Base processus zygomaticus
26	Tip processus zygomaticus
27	Most dorsolateral point processus paroccipitalis
28, 29c	Most ventral point processus paroccipitalis
30	Condylus occipitalis
31	Most caudal point cranium
32	Most rostromedial point vomer
33	Most medial connection between quadrate and skull (capitulum squamosum quadrati)

c, measured on contralateral side.

The number of cycles required for the algorithm to converge to accurate values (95% of the coordinates less than 0.002 mm from their true value) was estimated from a data set with known values and variance. After convergence of the algorithm the final set of values was averaged over all photographs to estimate the coordinates of the point measured.

Note that most points are not visible in all photographs. At least two photographs containing the landmark are required to estimate 3D coordinates, but the accuracy of the reconstructed coordinates will increase with the number of measurements available for a particular landmark (maximum N=7).

The overall s.d. after convergence for a stationary point was 0.052 mm (d.f.=705). However, after convergence the (pooled) s.d. for the rotating points was clearly higher. With an average number (3.9) of photographs showing a particular landmark, the standard error for the average x and y estimated is approximately 0.1 mm.

Morphometrics

Shape analysis was performed after a Generalised Procrustes Analysis (GPA) as

implemented in the program PAST (Hammer et al., 2001). The GPA superimposes sets of landmarks and removes variation in location, orientation and size between the skulls, using a least-squares fit technique (Rohlf and Slice, 1990; Bookstein, 1991). The GPA scales the size of the skulls to the average centroid size. The centroid size is the square root of the sum of the squared distances of a set of landmarks from their centroid (average).

The tpsSmall program (Rohlf, 1998) was used to determine whether the amount of variation in shape in the data set is small enough to permit statistical analyzes. This condition is met when there is a high correlation between the Euclidian distances between the configurations of the superimposed species and their corresponding Procrustes distance in the non-linear Kendall shape space. For our data set this correlation was very high (r=0.999).

The data from the Procrustes fit describe the shape differences among the skulls. These shape differences were quantified by means of a principal component analysis (PCA) of the covariance matrix in SPSS 10 (SPSS Inc., Chicago). The overall shape change of the skull was visualized through a thin plate spline analysis [tpsRelw (Rohlf, 2004)].

Univariate relationships between distances between landmarks and body mass were directly calculated from the 3D measurements. These distances were analyzed with the standardized major axis routine (S)MATR (v1) (Falster et al., 2003). This routine implements the algorithms developed by Warton and Weber (Warton and Weber, 2002).

Static bite force model

In order to determine the extent to which the differences in the shape of the skull between fringillids and estrildids result in differences in maximal bite force, we used a 2D static bite force model. The model calculates the position of all muscles and the lower jaw for a seed of a given diameter and at a given position in the beak, and finds the set of muscles force for which the bite force (force perpendicular to the upper beak) is maximal.

Although a large number of landmarks on the skull were measured, only a limited number of points are directly related to bite force (e.g. points defining the joints between neurocranium, quadrate, pterygoid, palatine and the jaws). Nine landmarks were used in the static force model and define the basic framework of the skull. Variation in their position may affect bite force directly. In the 2D model the joints between the bony elements of the skull are defined by x and y coordinates from the morphometric analysis (Fig. 3A; Table 2).

The jaw muscles were divided into eight groups, which are illustrated in Fig. 3B. For an extensive description of the jaw muscles in estrildids and fringillids see Nuijens and Zweers (Nuijens and Zweers, 1997).

The maximal force of jaw muscles was calculated from the muscle mass and fibre length using the formula:

$$F_{max} = m / (l\rho)M_c ,$$

where F_{max}=maximal muscle force (N); m=muscle mass (kg); l=mean fibre length (m); ρ=muscle density (1000 kg m^3); M_c=muscle stress constant [330 N m^2 (Hildebrand et al., 1985)].

Data on the xy coordinates of origin and insertion of muscles and muscle mass were not available for all species. We therefore estimated maximal muscle forces and muscle orientation for an average skull from the data of the morphometric analysis.

Jaw muscle weights for the average skull were calculated using the regression between total jaw muscle weight and centroid size. The estimated total jaw muscle weight was divided over the eight muscle groups according to the average percentage for each jaw muscle group as calculated from previously published data (van der Meij and Bout, 2004). Maximal forces were estimated by scaling down the fibre length for each muscle group measured in the greenfinch, using the relationship between centroid size and adductor fibre length (see van der Meij and Bout, 2004).

To remove the medially directed muscle force components for the 2D model a 3D analysis of directions of jaw muscles was made for the greenfinch by measuring the coordinates of the origin and insertion of all muscle groups (same procedure as for the landmarks of the skull). The orientations of the muscles of the greenfinch were fitted to the average skull by scaling the greenfinch down to the centroid size of the average skull and then the landmarks of the greenfinch skull were least-squares fitted to the landmarks of the average skull. After estimating the maximal bite force for the whole muscle the force components in the xy plane of the 2D static force model were calculated. The orientation and maximal force of all

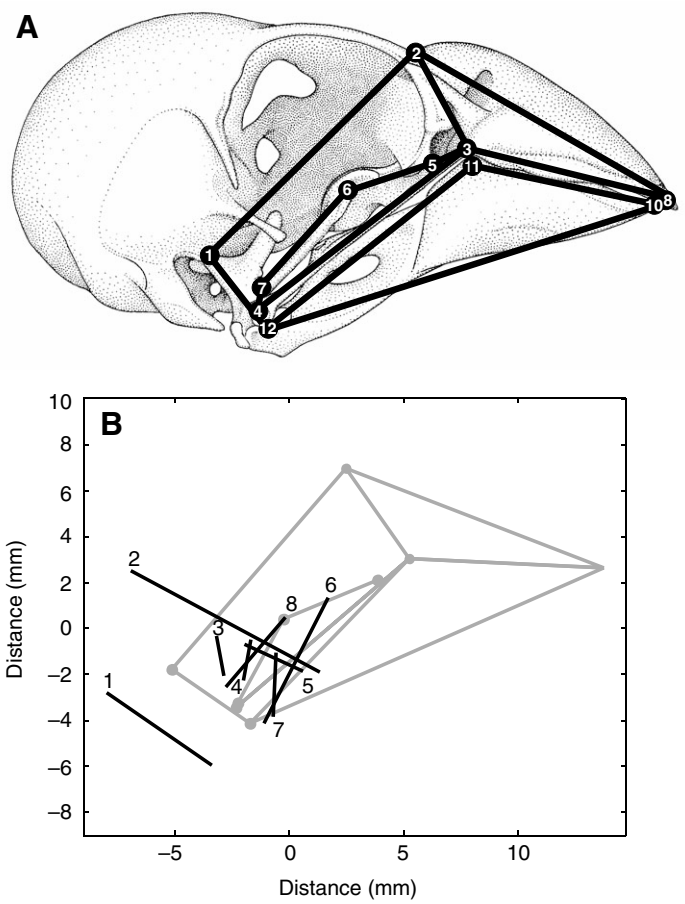

Fig. 3. The 2-D model of the avian skull, here illustrated by a spice finch adapted from Nuijens and Zweers (Nuijens and Zweers, 1997). (A) The skeletal points (1-12; see Table 2) of the model. (B) The bars connecting the model points (grey) and the muscle groups (black). 1, Musculus depressor mandibulae; 2, musculus adductor mandibulae externus and musculus pseudotemporalis superficialis; 3, musculus protractor quadrati; 4, musculus protractor pterygoidei; 5, musculus pseudotemporalis profundus and musculus adductor mandibulae ossis quadrati; 6, musculus pterygoideus ventralis and musculus pterygoideus dorsalis pars lateralis (all muscle fibre groups attached to the palatine); 7, musculus pterygoideus dorsalis pars medialis (muscle fibres attached to the pterygoid); 8, musculus retractor palatini. Axis labels represent distance of markers and muscles from centre of skull.

muscles were kept constant for all calculations involving skull shape comparisons.

The virtual seed (2 mm diameter) was positioned near the corner of the mouth (rictus=0) at 20% of the distance to the beak tip (=1). This position was roughly estimated from video recordings of birds trying to crack relatively hard seeds. The diameter going through the centre of the seed and the point where the seed touches the upper beak was kept perpendicular to the line defining the rim of the upper beak.

Finches have the ability to move their upper jaw relative to the braincase [prokinesis (Bock, 1964; Bühler, 1981; Zusi, 1984; Gussekloo et al., 2001)]. A somewhat different version of the static force model used to calculate bite force in the spice finch showed that bite force is slightly higher with elevated upper beak than with the upper beak in the resting position (Bout, 2002). This was not the case in our constructed average finch. All bite forces were therefore calculated with the upper beak in the resting position.

Bite forces were calculated under the assumption that muscles on both sides contribute to bite force. This was verified by EMG recordings.

Electromyography (EMG)

To verify model assumptions, the jaw muscle activity patterns (determined by EMG) during seed cracking were recorded in 11 Java sparrows. The birds were placed in a small box and kept under a steady flow of 0.3 l min^{-1} medicinal oxygen, and 0.4 l min^{-1} N_2O with 1.8 vol% isofluothane. After approximately 30 min the birds were transferred to the operating table. During the operation the gaseous mixture was administered through a plastic tube inserted into the beak and the amount of isofluothane was increased to 2.0 vol%. Bipolar measurements of muscle activity were made using eight 50 µm twisted, copper wire electrodes, positioned four on the left and four on the right side of each bird. For further details on the operation and the electromyography, we refer to Nuijens et al. (Nuijens et al., 1997). To measure the gape a magnetoresistive sensor (Philips KMZ10B, Eindhoven, The Netherlands) was glued on the upper bill. Opposite to the chip a small magnet was glued on the lower bill.

After recovery from the operation the birds were offered hemp seeds. During feeding the EMG signals were recorded with a 14-channel FM recorder [SE 700 tape recorder, S.E. Labs (EMI) Ltd., Feitham, UK] and stored on Ampex tape with a speed of 18.75 cm s^{-1}. The EMG signals were amplified 1000 times and high-pass filtered at 50 Hz.

After the experiments, the birds were sacrificed by an overdose of Nembutal, and the position of the electrodes was determined by dissection. The jaw muscles were divided into eight groups (see static bite force model section). For all groups the muscle activation patterns of one or more muscles were recorded, except for the very small M. retractor palatini. For EMG analysis the data were simultaneously digitized at a sample rate of 5000 Hz.

For each individual a number of cracking attempts were selected. The start and end of a cracking attempt were determined from gape measurements. The activity for each muscle during seed cracking was corrected for offset, full wave rectified, and distributed over a number of voltage classes. Maximum activity for each muscle was defined as the highest voltage class that occurred at least ten times among the data points. The EMG signal of each muscle was scaled to the maximal voltage measured.

Muscle activity was analyzed by multiplying the number of spikes (S) and the average amplitude (A) of the scaled data (Beach et al., 1982). S was calculated per interval of 20 data points (0.004 s).

RESULTS

Shape analysis

The mean skull configurations of a selected number of landmarks for fringillids and estrildids after Procrustes superimposition are shown in Fig. 4. The differences between landmarks for the average skull size of the two groups are between 0 and 0.6 mm. The variation between groups is much smaller than the variation within groups. Differences in landmark coordinates within groups vary between 0.5 and 3.5 mm.

Our data set consisted of more variables (33 points in 3D=99) than species (N=42), so it was not possible to test the effect of size and family on shape directly. To reduce the dimensionality a principal component analysis (PCA) was performed on the variance–covariance matrix of the Procrustes-fitted coordinates of all the species. The PCA allowed us to take into account the correlation among coordinates of landmarks. The effects of group (estrildid *vs* fringillid) and body size (3D centroid size) were tested by a multivariate GLM over the first 17 principal components (PCs) of the 3D data, which retained 90% of the shape variance. Both factors were highly significant (group: $F_{17,23}$=12.60, P=6.97×10^{-8}; centroid size: $F_{17,23}$=17.96, P=2.03×10^{-9}). Most of the variation related to group and centroid size is described by the first three PCs, which explain 26.4%, 13.7% and 9.6% of the total shape variation, respectively (total 49.7%). Subsequent PCs are mostly related to differences between species.

As we intend to relate shape differences to bite force through a 2D static bite force model we repeated the analysis with just the xy coordinates. The results of the 2D analysis were very similar to the 3D results. The components of the 2D PCA were used as input for the bite force model.

Principal components

The overall shape change of the skull was visualized through a thin plate spline analysis (Fig. 5). For the parameters chosen (all principal warps included and given the same weight) this analysis is equivalent to a PCA of the Procrustes-fitted landmark coordinates.

The first PC (or so-called relative warp) shows variation in the expansion of the area in front of the quadrate, in the dorsoventral position of the kinetic hinge of the upper beak and the orbit, and variation in the length of the neurocranium behind the quadrate (Fig. 5A). This variation in shape is related to differences in body size. The factor scores of PC1 are negatively correlated with 2D-centroid size for both estrildids (r=–0.686, N=22, P=0.000) and fringillids (r=–0.814, N=20, P=0.000). Standardized major axis analysis shows that the slope (P=0.535) and intercept (P=0.070) of the relationship between factor scores and centroid size is similar for the two groups of finches (Fig. 6, PC1).

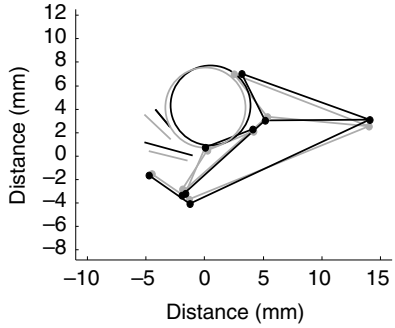

Fig. 4. Mean skull configuration of a selected number of landmarks for fringillids (black) and estrildids (grey) after superimposition.

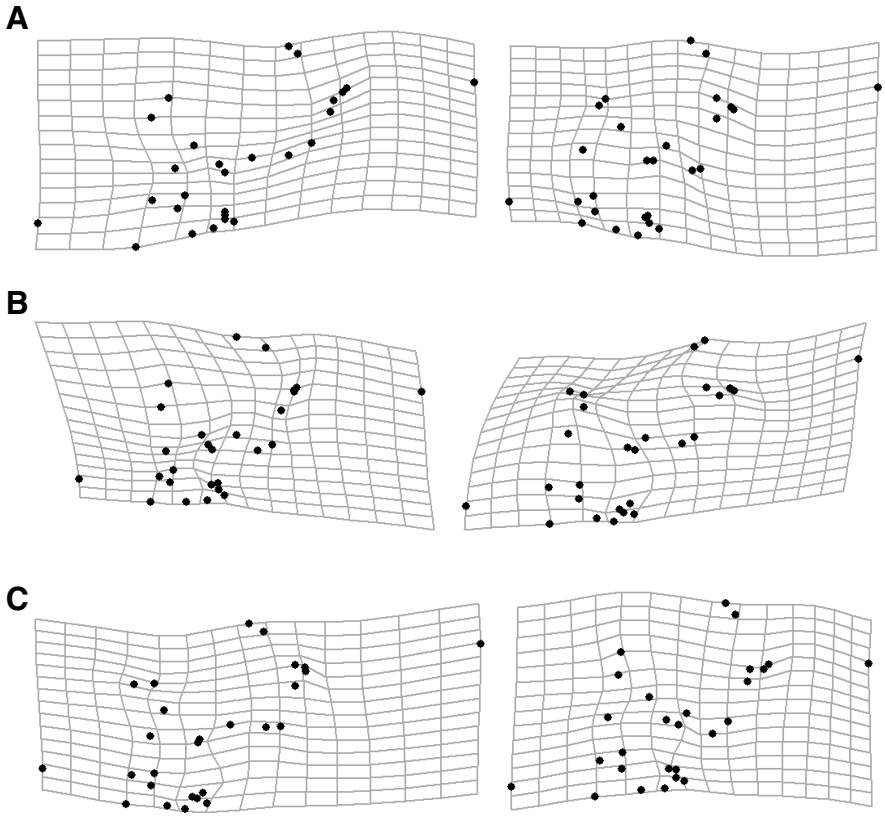

Fig. 5. Thin plate spline representation of principal trends (relative warps) in the variation of the shape of the skull for fringillids and estrildids. Grids show the deformation of the average shape in opposite directions of the first three relative warps (A–C).

The factor scores of PC2 are correlated with 2D-centroid size for both estrildids (r=0.647, N=22, P=0.001) and fringillids (r=0.566, N=20, P=0.009), but the slope (P=0.000) and intercept (P=0.000) differ considerably. While the scores are very low over the whole range of head sizes in fringillids, they increase strongly with head size in estrildids (Fig. 6, PC2). Therefore this factor represents a change in shape that is more or less typical of estrildids. PC2 is characterized by (co)variation in the position of the frontonasal hinge and orbit, by variation in the angle of the beak with respect to the neurocranium, and by variation in the length and the position of the postorbital process and the position of the zygomatic process (Fig. 5B). A more downward inclined beak is associated with a more dorsocaudal position of the frontonasal hinge (Fig. 7). For the Procrustes fitted coordinates the x coordinate of the frontonasal hinge (P=0.013) and the y coordinate of the beak tip (P=0.008) are significantly smaller in estrildids than in fringillids.

The expansion of the area in front of the quadrate reflects the positive allometric increase in size of a number of structures: the length of the quadrate itself, its processus protruding into the orbit, the processus zygomaticus and processus postorbitalis, and the pterygoid (Table 3). The base and tip of the processus zygomaticus and processus postorbitalis also move upward and forward with respect to the quadrate. Consequently, the distance from the articulation between quadrate and skull to the base of the processus postorbitalis also increases positively allometrically.

The expansion of the area of the quadrate is accompanied by a dorsal shift of the orbit. The increase in the size of the orbit with body size does not differ significantly from isometrical. Together with the orbit the frontonasal hinge moves upward and its height measured with respect to the palatine increases positively allometrically with head/body size.

The jugal bar, which borders the orbit ventrally, also increases isometrically in length with increasing body size. The length of the palatine, which is also partly situated below the eye, is highly variable. Its increase in length is also consistent with isometry. However, the transpalatine process connected to the main body of the palatine shows a strong positive allometric increase in length. The (3D) lengths of pterygoid and palatine are negatively correlated when (3D) centroid size is held constant (log-transformed, r=–0.310, P=0.048, d.f.=39). The connections of both the palatine and jugal with the upper beak shift backward with increasing head/body size (Fig. 7).

The positive allometric increase in size of structures in the area of the quadrate is in marked contrast to the length of the neurocranial part of the skull behind the quadrate. The length of this part of the skull, measured between the processi paroccipitalis and either the condylus occipitalis or the most caudal point of the skull, increases negatively allometrically with size (Table 3).

The distance between the quadrate and the base of the processus zygomaticus, and to a lesser extent the distance between the quadrate and the processus postorbitalis, decreases and partly reduces the effect of strong positive allometric expansion in this area (PC1). The palatine becomes relatively shorter in estrildids than in fringillids with increasing head/body size.

The factor scores of PC3 are only very weakly correlated with head size (Fig. 6, PC3). In estrildids the correlation is not significant (r=–0.211, P=0.345, N=22), while in fringillids the correlation is significant but weak (r=–0.506, P=0.023, N=20). PC3 mainly describes differences in beak length that covary with the height of the frontonasal hinge and orbit (Fig. 5C). When the beak is relatively long the height of the hinge and orbit are small. The connections of both palatine and jugal with the upper beak shift backward when the beak is long (Fig. 7).

While much of the variation in shape is related to size, some differences between estrildids and fringillids are present. As the slope and intercept for the factor scores of PC1 are similar for both groups of finches the main differences between estrildids and fringillids are described by PC2 and PC3. There are no systematic differences in the length of the quadrate, the processus orbitalis, the pterygoid or the palatine. The processus zygomaticus, however, is significantly longer and the processus postorbitalis is shorter in fringillids than estrildids (Table 3; PC2). The base of the processus zygomaticus is situated at a larger distance from the quadrate in fringillids than in estrildids (Fig. 4; Table 3; PC2). Estrildids also have more downward inclined (PC2) and longer beaks than fringillids of the same size (Table 3; PC3).

Bite force calculations

The effect of the principal components on the maximal bite force has been determined with a static bite force model. To determine

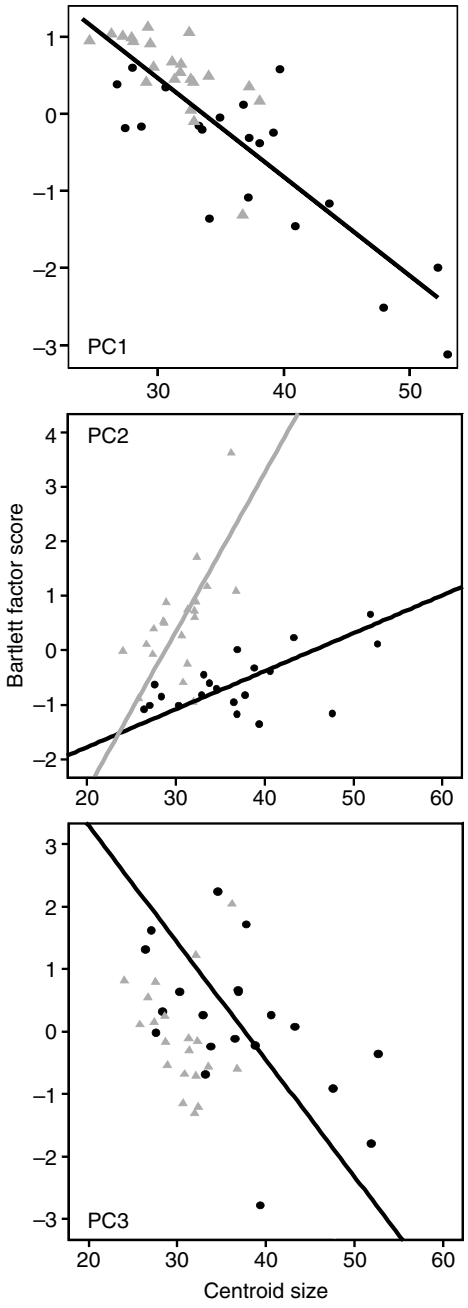

Fig. 6. The relationship of PC factor scores with centroid size. Black circles, fringillids; grey triangles, estrildids.

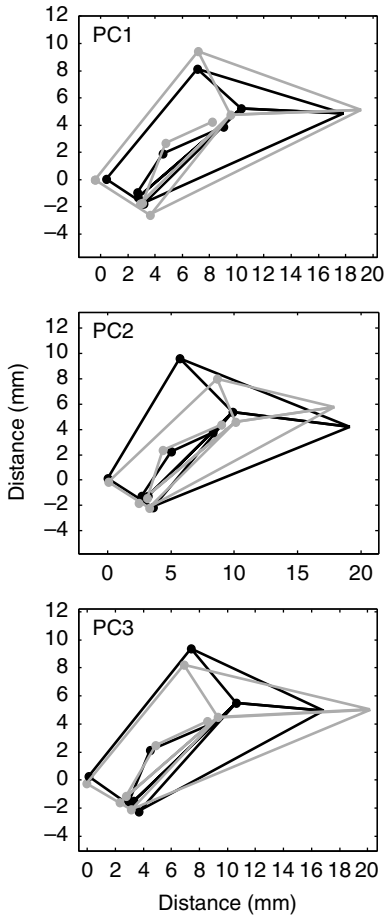

Fig. 7. The effect of the first three principal components (PC1–3) on the configuration of skull landmarks used for the static force model. The configuration of the skull in the positive direction is represented in black, in the negative direction in grey. The change has the same magnitude for each PC and does not represent the measured variation but was chosen for graphical purposes only. Axis labels represent distances with respect to the centroid of the measured skull points.

the effect of skull shape on bite force we calculated the maximal bite force for two landmark configurations per principal component. These two landmark configurations were calculated as the average landmark configuration plus or minus the vector describing the principal component (arbitrarily) standardised to length 3. The effect of the three PCs on the configuration of the modelled skull is shown in Fig. 7.

All three components show variation in bite force as a result of changes in the configuration of skull elements. The first principal component represents a pattern of (allometric) shape changes that correlates with skull size. As head/body size increases the change in shape of the skull elements results in an increase in bite force (Table 4) in both fringillids and estrildids. An analysis of the contribution of single landmarks to the change in bite force that results from the whole suite of changes described by PC1, shows that the change in bite force is almost completely due to the shift in the position of the quadrate. The change in bite force for the other landmarks is relatively small: 0–3% of the bite force for the average finch (11.5 N). These small changes in landmarks that covary along PC1 may increase or decrease bite force. The more dorsal position of the kinetic hinge and more ventral position of the joint between quadrate and pterygoid for instance, increase the force that may be exerted by the upper jaw, while at the same time the dorsal shift of the palatine decreases the bite force of the upper beak.

The suite of shape changes described by PC2 result in a variation in bite force similar in magnitude to the variation calculated for PC1 (Table 4). As in PC1 the changes in bite force are the result of a single character. In PC2 a more downward inclined beak increases bite force. The shifts of other landmarks result in increases or decreases in bite force of the upper beak that are much smaller than the effect of beak angle. A more dorsocaudal position of the frontonasal hinge has a small positive effect on bite force, while for instance the associated dorsal shift of the joint between quadrate and pterygoid has a negative effect.

Table 3. Relationships between log-transformed skull measurements and body mass

		N	r^2	Slope	*P*-1	95% CI	Int. com. slope	*P*-2
Length pr. zygomaticus	F	20	0.599***	0.534		0.392–0.727	–0.038	
	E	22	0.258*	0.521	0.921	0.352–0.771	–0.096	0.026
	C	42		0.529		0.420–0.666		
Length pr. postorbitalis	F	20	0.297*	0.538		0.359–0.807	–0.572	
	E	22	0.513***	0.800	0.123	0.581–1.102	–0.330	0.000
	C	42		0.688		0.546–0.871		
Dist. otic joint quadrate (5) to pr. postorbitalis (27)	F	20	0.790***	0.445		0.355–0.557	0.008	
	E	22	0.563***	0.477	0.704	0.352–0.646	0.030	0.091
	C	42	0.770***	0.486		0.417–0.566	0.132	
Dist. otic joint quadrate (5) to pr. zygomaticus (29)	F	20	0.625***	0.556		0.412–0.749	–0.222	
	E	22	0.188*	0.535	0.885	0.352–0.815	–0.338	0.000
	C	42		0.549		0.434–0.695		
Length quadrate	F	20	0.908***	0.570		0.491–0.661	–0.048	
	E	22	0.561***	0.483	0.327	0.357–0.655	–0.043	0.761
	C	42	0.841***	0.542		0.477–0.616	–0.032	
Length pr. orbitalis quadrati[c]	F	20	0.863***	0.491		0.409–0.590	0.008	
	E	22	0.643***	0.510	0.813	0.388–0.672	0.030	0.707
	C	42	0.832***	0.521		0.457–0.593	–0.011	
Length pterygoid	F	20	0.922***	0.483		0.420–0.554	0.106	
	E	22	0.668***	0.478	0.952	0.367–0.624	0.102	0.761
	C	42	0.874***	0.486		0.434–0.544	0.098	
Length palatine	F	20	0.121	0.330		0.211–0.517	0.241	
	E	22	0.132	0.332	0.985	0.218–0.506	0.225	0.490
	C	42	0.255**	0.349		0.266–0.458	0.211	
Length pr. transpalatinus[b]	F	20	0.826***	0.645		0.526–0.792	–0.312	
	E	22	0.473***	0.659	0.914	0.473–0.919	–0.348	0.115
	C	42	0.766***	0.691		0.592–0.806	–0.382	
Length jugal	F	20	0.713***	0.305		0.235–0.396	0.615	
	E	22	0.727***	0.336	0.571	0.264–0.428	0.599	0.139
	C	42	0.772***	0.335		0.288–0.390	0.590	
Orbit diameter	F	20	0.885***	0.355		0.300–0.419	0.439	
	E	22	0.478***	0.351	0.946	0.252–0.488	0.450	0.604
	C	42	0.795***	0.348		0.301–0.402	0.451	
Length caudal neurocranium[a]	F	20	0.450**	0.228		0.159–0.326	0.424	
	E	22	0.547***	0.251	0.681	0.184–0.341	0.480	0.000
	C	42		0.241		0.192–0.302		
Length cranium external	F	15	0.894***	0.365		0.301–0.443	0.787	
	E	22	0.481***	0.347	0.778	0.257–0.468	0.772	0.256
	C	41	0.795***	0.376		0.325–0.435	0.759	
Dist. med. (6) to lat. (7) condyle quadrate	F	20	0.918***	0.455		0.395–0.524	–0.261	
	E	22	0.662***	0.490	0.629	0.375–0.640	–0.309	0.000
	C	42		0.462		0.404–0.528		
Length upper beak[d]	F	20	0.846***	0.627		0.517–0.760	0.161	
	E	22	0.581***	0.554	0.472	0.411–0.746	0.206	0.021
	C	42		0.605		0.518–0.707		
Width skull at pr. paroccipitalis	F	20	0.779***	0.280		0.222–0.352	0.551	
	E	22	0.638***	0.388	0.069	0.294–0.511	0.559	0.517
	C	42	0.756***	0.309		0.264–0.362	0.567	
Width skull at joint quadrate–pterygoid	F	20	0.780***	0.322		0.256–0.406	0.433	
	E	22	0.564***	0.366	0.509	0.270–0.495	0.430	0.810
	C	42	0.760***	0.339		0.290–0.396	0.429	
Width skull at connection jugal–upper beak	F	20	0.906***	0.576		0.496–0.670	0.085	
	E	22	0.670***	0.598	0.798	0.459–0.780	0.083	0.873
	C	42	0.863***	0.585		0.520–0.658	0.079	
Width beak external	F	16	0.875***	0.631		0.516–0.771	0.027	
	E	26	0.580***	0.639	0.939	0.488–0.837	0.087	0.007
	C	42		0.633		0.539–0.744		
Height frontonasal hinge[e]	F	20	0.835***	0.535		0.438–0.654	–0.050	
	E	22	0.226*	0.703	0.228	0.471–1.048	–0.001	0.056
	C	42	0.582***	0.545		0.444–0.670	–0.003	
Height beak external	F	16	0.936***	0.637		0.553–0.734	0.001	
	E	26	0.659***	0.732	0.321	0.574–0.934	0.038	0.060
	C	42	0.636***	0.636		0.559–0.723	0.050	

F, fringillids; E, estrildids; C, all species; *N*, number of species; r^2, coefficient of determination; *P*-1, probability of a common slope; CI, confidence interval slope; Int. com. slope, intercept for common slope; *P*-2, probability of a common intercept for the common slope.

[a]Length in the medial (*xy*) plane between landmarks 27 and 31.

[b]Average length of distance between landmarks 15/14 and 18/19.

[c]Distance from tip of process (landmark 9) perpendicular to the long axis of the quadrate (landmarks 5–6).

[d]Distance in the medial (*xy*) plane between upper beak tip (landmark 4) and (the projection of) the connection jugal–upper beak (landmark 20).

[e]Distance along *y* between frontonasal hinge (landmark 3) and connection palatine–upper beak (landmark 19).

Asterisks indicate significant levels: *P<0.05, **P<0.01, ***P<0.001.

The variation in bite force associated with the shape changes described by PC3 is slightly more complex. With increasing head/body size the relative length of the beak increases, the height of the frontonasal hinge decreases, and the quadrate shifts caudally. These shape changes increase bite force (Table 4). Part of the increase in bite force comes from the caudal shift of the quadrate, as in PC1. The other part comes from the shortening of the palatine and jugal.

When the seed is kept in the same position as in an average finch, changing the position of the beak tip has no effect on bite force. The position of the connection of the jugal with the upper beak, however, does have an effect. In finches the position of this connection is indicative of the position of the corner of the mouth (rictus). There is a high correlation between the external length of the beak of the intact animal measured between rictus and beak tip, and the length of the beak measured on the skull between the connection jugal–upper beak and beak tip (r=0.945, N=19). When palatine and jugal become shorter but the position of the seed remains unchanged bite force becomes lower. However, when the rictus moves caudally with the connection between jugal and upper beak, the seed may also move caudally to stay at the same (absolute) distance to the rictus. When the seed also moves caudally bite force increases strongly.

EMG

A representative example of the EMG activity of a number of jaw muscles during seed cracking is shown in Fig. 8. There is no difference between EMG activity during successful and unsuccessful cracking attempts (not shown here). Muscles on the right side and left side of the bird show very similar activation patterns.

A cracking attempt starts with a very small amplitude closing movement (vertical line 1 in Fig. 8), followed by re-opening before the actual cracking starts (vertical line 2 in Fig. 8). During re-opening only the upper and lower jaw openers are active. When jaw opener activity decreases the jaws start to close for the actual cracking attempt starts. During the cracking attempt the adductors inserting on the quadrate, the adductors of the lower jaw and the pterygoid muscles are all active. The amplitude of the muscle activity increases until the seed cracks or until the cracking attempt is terminated. When adductor and pterygoid activity decreases the jaws start to open again (vertical line 3 in Fig. 8). There is some low level activity of the protractor of the quadrate (upper jaw openers) during a cracking attempt.

DISCUSSION

Fringillids and estrildids differ in their husking performance on hard closed-shelled seeds. The time required to crack a seed is directly related to seed hardness and to maximal bite force (van der Meij et al., 2004; van der Meij and Bout, 2006). In a previous study (van der Meij and Bout, 2004) we showed that there is a significant difference in jaw muscle mass and maximal bite force between fringillids and estrildids. Fringillids have relatively larger jaw muscles than estrildids and are able to produce higher bite forces than estrildids of the same body size. Compared to other birds the jaw muscles of both fringillids and estrildids scale positively allometrically with body size.

Differences in maximal bite force within and between taxa may depend not only on differences in jaw muscle forces, but also on differences in the geometry of the cranial elements that affect lever arms. A high upper bill (kinetic hinge), for instance, is often interpreted as an adaptation to large bite force because it increases the moment of the upper jaw closing muscles (Bowman, 1961; Bock, 1966). Without a biomechanical analysis, however, interpretations of changes in shape of the skull remain hazardous, because differences in skull morphology may not only be related to variation in bite force, but also to variation in the attachment area for jaw muscles or to differences in the resistance to joint reaction forces, or could be the consequence of changes in the shape or position of neighboring structures.

Table 4. The effect on bite force of the first three principal components describing shape variation in estrildids and fringillids

	Bite force (N) for PC-length	
	–3	+3
PC1	12.5	10.4
PC2	10.7	12.6
PC3	12.4	11.3

Skull configuration and maximal bite force

The analysis of the relationship between the position of landmarks and bite force suggests that only a few changes are directly related to bite force. Most differences in landmarks that are present in the static force model result in small changes in bite force, and only three characters have a large impact on bite force: a caudal shift of the quadrate (PC1), a downward inclination of the beak (PC2) and a caudal shift of the rictus (PC3).

Lengthening of the quadrate leaving its orientation and all muscles unchanged by itself does not increase bite force, but a more caudal position of the quadrate does increase the lever arm of jaw closer muscles. Large billed Geospizinae species also have a more posterior position of the quadrate than small-billed species (Bowman, 1961). However, the increase in lever arm is not independent of muscle size. The expansion of the area around the quadrate with increasing head/body size (PC1) is related to the positive allometric increase of jaw muscle size with body size. The processus zygomaticus and processus orbitalis of the quadrate serve as (musculous) attachment area for jaw closer muscles, while a large part of the upper jaw closers attach to the pterygoid and to the transpalatine process. Jaw muscle mass increases so fast with body size (body mass$^{1.29}$) that the linear dimensions of attachment areas have to increase with an exponent of 0.43. As a result of the positive allometric increase of skull dimensions in the jaw closer attachment area, the processus orbitalis becomes longer and the quadrate shifts backwards. This leaves the origo and insertion of the quadrate adductors approximately the same and increases the lever arm of the quadrate adductors. The increase in skull dimensions around the quadrate also affects the position of the processi zygometicus and postorbitalis. These processi, which border the orbit, move upwards. Consequently, when the diameter of the eye and orbit has to remain the same, the orbit has to move upward too.

The increase in the area for muscle attachment does not seem to affect skull width. The distances between left and right processus paroccipitalis just behind the ear and between the left and right quadratopterygoid joints increase isometrically (Table 3). A strong relationship between head width and bite force has been found in Darwin's finches (Herrel et al., 2005b). However, we did not find any difference in skull width between fringillids and estrildids. As the external head measurements in Darwin's finches include the voluminous jaw muscles, differences in relative head width as found in Darwin's finches may reflect differences in relative jaw muscle size (and therefore bite force) rather than differences in skull width.

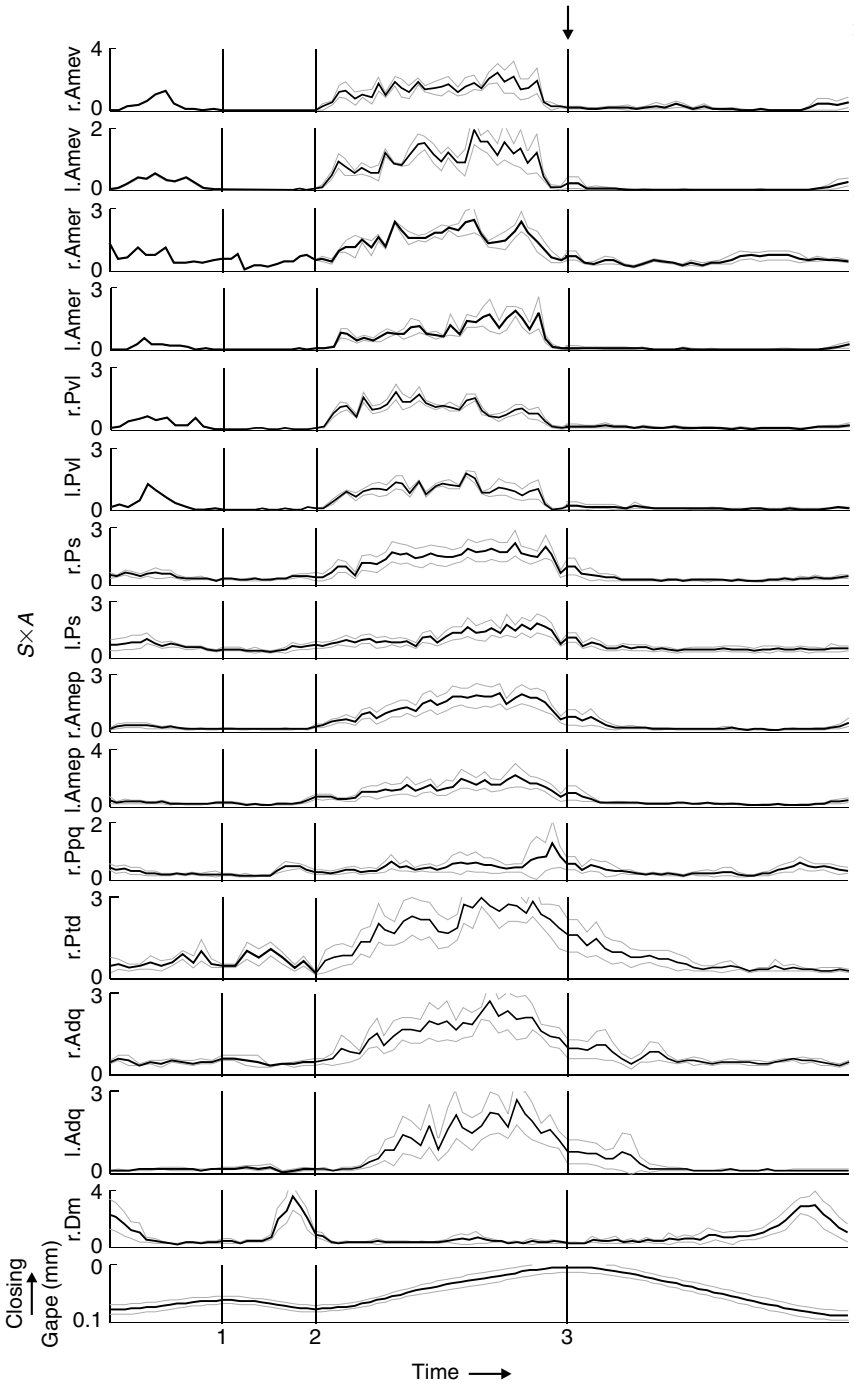

Fig. 8. Average EMG and standard deviation (grey lines) of the jaw muscles during seed cracking attempts in the Java sparrow (composite of three experiments). Muscle activity is expressed as the number of spikes $S \times$ mean amplitude A per time bin; gape in mV. The time axis is standardized to the average duration of the phases, in order to average muscle activity over a large number of cracking attempts (67–159). Vertical lines 1–3 mark the transitions between beak closing (up in bottom trace) and opening movements (down). Arrow indicates end of beak closing phase. Abbreviations: l, left; r, right side; Ame, M. adductor mandibulae externus with a posterior, rostral and ventral part; Adq, M. adductor mandibulae os quadrati; Dm, M. depressor mandibulae; Ppq, M. protractor pterygoideus et quadrati; Ps, M. pseudotemporalis superficialis; Ptd, M. pterygoideus dorsalis; Pvl, M. pterygoideus ventralis.

The change in bite force that is associated with PC2 is largely the result of the change in angle between the beak and the skull. In estrildids the beak becomes much more inclined downward with increasing skull size (e.g. *Pyrenestes sanguineus*) than in fringillids. The increase in bite force with a more downward inclined beak is caused by the small decrease in distance between the seed and the jaw muscles. Why the downward inclination of the beak is so much more pronounced in estrildids than in fringillids is not clear. Increasing jaw muscle mass (see below) may be much more effective for increasing bite force than shape changes of the skull. Alternatively, an increase in jaw muscle mass may be constrained in estrildids and shape changes may be the only option to increase bite force.

Many of the changes associated with a more inclined beak in estrildids seem to be related to the difference in jaw muscle size between estrildids and fringillids. Jaw muscle mass is approximately 0.67 times lower in estrildids than in fringillids of the same size (van der Meij and Bout, 2004). Consequently, estrildids require less space between the quadrate and orbit for their jaw closer muscles. In estrildids the zygomatic and postorbital process are situated closer to the quadrate and the distance between the quadrate and orbit is therefore smaller in estrildids than in fringillids. The smaller length of the zygomatic process (PC1) in estrildids may also be related to the difference in jaw muscle size between the two groups. However, some of the other processi or bones to which jaw muscles attach do not differ in length between estrildids and fringillids (pterygoid, pr. orbitalis, pr. transpalatinus), while the inserting muscles do differ in size.

The third potentially beneficial shape change that increases bite force is a caudal shift of the rictus to create a shorter work arm for the jaw closer muscles. This is especially clear in large fringillids (*Eophona*, *Coccothraustes*, *Mycerobas*). Although variation in the position of the connections of jugal and palatine with the upper beak does occur, this variation is limited, possibly by spatial constraints. In finches the distance between the beak and eye is much smaller than in many other species. A large decrease in the distance between beak and the jaw closing muscles to get a shorter work arm with increasing body size may not be possible because the eye and muscles occupy all the space between the beak and quadrate. In estrildids there is no significant correlation between the position of the connections between jugal and palatine with the upper beak (PC3) and head/body size. Unfortunately, the range of body mass in estrildids is limited because, unlike fringillids, there are no estrildids with a body mass over 40 g. This makes it difficult to establish the relationship with certainty. The larger variation in the position of jugal and palatine connections with the upper beak in fringillids may represent species-

specific shape differences and not be related to differences between the two groups of finches.

Other landmarks

Contributions to bite force from the variation of other landmarks, e.g. a dorsal shift of the frontonasal hinge, are not only relatively small compared to the effect of the main shape changes, but also covary with changes in landmarks that effect bite force negatively. The relatively small contribution of some of the landmarks is not just because the observed changes differ in magnitude. Lowering the beak tip or raising the frontonasal hinge over the same distance, for instance, shows that changing the position of the frontonasal hinge is far less effective than changing the angle of the beak. The covariation of differences in landmarks that affect bite force positively or negatively is surprising because when there is a strong selection on large bite force one would not expect to find shape changes that contribute to a decrease in bite force. This makes it difficult to understand the functional significance of an increase in bill height (frontonasal hinge). In finches the cranium is relatively short compared to many other birds with relatively smaller jaw muscles (e.g. anseriformes, unpublished observations) and the frontonasal hinge directly borders the dorsoanterior part of the orbit. In many other species the frontonasal hinge is more in front of the orbit. The position of the frontonasal hinge close to the orbit suggests that the hinge may shift upward with the orbit as a consequence of the expansion of the jaw closer attachment area. An increase in bite force is not always associated with a higher beak (PC1). In PC3 an increase in bite force is associated with a more ventrally positioned hinge. Alternatively, variation in the height of the frontonasal hinge may be related to the reaction force in the hinge. Model calculations show that the reaction force in the hinge decreases for the same bite force as its height increases. As finches evolve stronger jaw muscles and larger bite forces, corresponding changes in beak height may be required to avoid structural failure of the very thin flexible zone of the kinetic hinge (see also Herrel et al., 2005b).

A similar explanation may hold for the changes in the pterygoid/palatine chain that are associated with a more caudal position of the quadrate with increasing head size (PC1). The combined effect on bite force of the relative shortening of the palatine, a more dorsal position of the palatine, and the more ventral position of the quadrate–pterygoid joint is negligible, but the reaction forces in the perygoid–palatine joint, the quadrate–pterygoid joint and the connections of the jugal all become relatively smaller, compared to a model skull with just a more caudally positioned quadrate. The reaction force in the connection between palatine and upper beak, on the other hand, increases.

Interestingly, the shape changes in the pterygoid–palatine chain associated with the more posterior position of the quadrate (PC1) are partly reversed in PC2: the quadrate–pterygoid joint is positioned more dorsally, and the palatine becomes relatively longer. This increases joint reaction forces in estrildids (see before) compared to fringillids when bite force is the same, but jaw muscles and maximal bite force are systematically smaller in estrildids than in fringillids. Therefore, reaction forces may in fact be similar for birds of the same size.

Model calculations and EMG

To assess differences in skull shape the size and orientation of muscles is kept constant in the model. Whether there are differences in muscle orientation between taxa was not investigated as the centres of origin and insertion of muscles may only be roughly estimated. Although muscle orientation seems very similar across species, small changes in muscle orientation may have a large effect on bite force.

For the calculation of maximal muscle forces it is assumed that the muscles on both sides of the head contribute to bite force. The EMG recordings show that left and right jaw muscles are approximately active at the same time and with the same amplitude during cracking. This muscle activation pattern is in good agreement with the results predicted by the model for maximal bite force. Low-level activity of the protractor muscles in the model critically depends on the position of the seed along the beak but is also predicted for submaximal bite forces. The activity of the very small retractor palatini could not be verified.

Differences between fringillids and estrildids

The analysis of landmarks representing the basic shape of the skull shows that, although there are small but significant differences between some of the landmarks, the difference between the two families is small compared to interspecific variation. The relationship between log jaw muscle mass and log bite force for the two taxa described previously (van der Meij and Bout, 2004) already explains 88% of the variation in bite force. Most of the total variation in skull geometry (approximately 78%) represents differences in size, which leaves very little variation in bite force to be explained by differences in shape between the two groups of finches.

Static bite force calculations show that the effect of the difference in average shape between fringillids and estrildids is small. An average fringillid skull has a slightly higher bite force (0.5 N) than an average estrildid skull for the same muscle sizes and configuration. This difference is very small compared to the effect of the smaller jaw muscle mass in estrildids (van der Meij and Bout, 2004). Jaw muscle mass is approximately 0.67 times lower in estrildids than in fringillids of the same size. For the calculated maximal bite force of the average estrildid in the present study this amounts to a decrease in bite force of approximately 4.0 N.

The comparison of bite force between the average skull configurations of the two taxa, however, is biased because the fringillids in our samples are larger than the estrildids. When the three largest fringillids are removed (*Mycerobas*, *Coccothraustes*, *Eophona*) to make average body weight comparable, the caudal shift of the quadrate and the connection between jugal and upper beak disappear. Surprisingly, the shape of the unbiased average fringillid skull is less suited to generate bite force than the shape of the average estrildid skull: bite force is lower (11.1 *vs* 11.9 N) for the fringillid skull than for the estrildid skull. The higher bite force of the estrildid skull is almost completely the result of the more depressed angle of the bill. For an average estrildid skull with the beak elevated to the same position as in the average fringillid the bite force is 1.0 N lower.

The frontal nasal hinge has a more rostral position in fringillids than in estrildids. The difference is small (0.6 mm) and model calculations show that this difference contributes very little to bite force. Similarly, the small differences in the position of the joint between the pterygoid and the quadrate, the connection between the pterygoid and palatine, and the connection between the jugal bar and the quadrate contribute very little to bite force. Many other differences between the two groups of finches do not contribute to bite force directly, but only indirectly through the positive allometric growth of the jaw muscles (e.g. the length and position of processi serving as attachment area), or may be related to the consequences of large bite forces or to the way seeds are cracked.

Several studies have shown that bite force is correlated with beak height and width (Herrel et al., 2005b), and that there are performance and fitness advantages for birds with deep and wide beaks in cracking hard seeds (Grant and Grant, 1995; Grant and Grant, 1999; Benkman, 2003). In our study a strong positive allometric increase in jaw muscle mass and bite force with body mass (Van der Meij and Bout, 2004) is associated with a positive allometric increase in both height and width of the beak in both groups of finches. Bite force in estrildids is only 71% of similar sized fringillids and one would therefore expect the relatively large difference in bite force to be reflected in differences in beak height and width. Beak height, however, is only close to significance, possibly because the range of body sizes of the birds in this study is small. Beak width measured as the distance between the connections of jugal and upper beak is not different for the two groups of finches. Beak width measured externally, including the ramphotheca, on the other hand is clearly different. Apparently, the width of the ramphotheca is larger in fringillids than in estrildids. Larger bite forces in fringillids allow birds to crack harder seeds. As seed hardness and seed size are correlated (Abbott et al., 1977; Van der Meij and Bout, 2000) one would expect a wider husking groove in the ramphotheca of fringillids to efficiently crack the larger seeds (Benkman, 1993; Benkman, 2003).

Both height and length of the bill increase positively allometrically with body size and tend to be larger is estrildids than in fringillids, but there is a large variation within the two groups. It has been shown that beak length is controlled independently from beak height and width during development (Abzhanov et al., 2006).

In fringillids the distance between the lateral and medial condyle of the joint between the quadrate and mandible is larger than in estrildids. This increases the articular surface of the quadrate with the mandible and may be an adaptation to large compression forces in the quadratomandibular joint (Bowman, 1961). A broad quadratomandibular joint may also contribute to stability of the joint during powerful adduction (Bowman, 1961) or be related to the large lateral lower jaw movements during seed handling in fringillids, which are absent in estrildids (Ziswiler, 1965; Abbott et al., 1975; van der Meij and Bout, 2006).

In summary we conclude that most morphological variation related to bite force among the granivorous species of the Fringillidae and Estrildidae is confined to size. As bite force is largely determined by jaw muscle size and jaw muscles scale positively allometrically with body size in both groups, selection for high bite force more or less coincides with selection for body size.

The contribution of variation in shape to bite force is modest, largely size dependent and similar in estrildids and fringillids. Only one character clearly contributes to the difference in bite force independent of size: the angle of depression of the bill. The bill is inclined downward more in estrildids than in fringillids. This shape difference results in a slightly higher bite force but does not compensate for the much smaller jaw muscle size in estrildids. The variation in the position of other landmarks is related to muscle size or may be related to the reduction of reaction forces in the jaw apparatus.

We wish to thank Wouter van Gestel from Wageningen University for help with collecting the species and M. Heijmans of the technical department of our institute for constructing the rotating device.

REFERENCES

Abbott, I., Abbott, L. K. and Grant, P. R. (1975). Seed selection and handling ability of four species of Darwin's finches. *Condor* **77**, 332-335.

Abbott, I., Abbott, L. K. and Grant, P. R. (1977). Comparative ecology of Galapagos ground finches (*Geospiza* Gould): evaluation of the importance of floristic diversity and interspecific competition. *Ecol. Monogr.* **47**, 151-184.

Abzhanov, A., Kuo, W. P., Hartmann, C., Grant, B. R., Grant, P. R. and Tabin, C. J. (2006). The calmodulin pathway and evolution of elongated beak morphology in Darwin's finches. *Nature* **442**, 563-567.

Arnold, S. J. (1991). Constraints on phenotypic evolution. *Am. Nat.* **140S**, 85-107.

Beach, J., Gomiak, G. C. and Gans, C. (1982). A method for quantifying electromyograms. *J. Biomech.* **15**, 611-617.

Benkman, C. W. (1993). Adaptation to single resources and the evolution of Crossbill *(Loxia*) diversity. *Ecol. Monogr.* **63**, 305-325.

Benkman, C. W. (2003). Divergent evolution drives the adaptive radiation of Crossbills. *Evolution* **57**, 1176-1181.

Björklund, M. (1991). Patterns of morphological variation among cardueline finches (Fringillidae: Carduelinae). *Biol. J. Linn. Soc. Lond.* **43**, 239-248.

Björklund, M. and Merilä, J. (1993). Morphological differentiation in *Carduelis* finches: adaptive vs. constraint models. *J. Evol. Biol.* **6**, 359-373.

Boag, P. T. and Grant, P. R. (1981). Intense natural selection in a population of Darwin's finches (Geospizinae) in the Galapagos. *Science* **214**, 82-85.

Bock, W. J. (1964). Kinetics of the avian skull. *J. Morphol.* **114**, 1-42.

Bock, W. J. (1966). An approach to the functional analysis of the bill shape. *Auk* **83**, 10-51.

Bookstein, F. L. (1991). *Morphometric Tools for Landmark Data: Geometry and Biology*. New York: Cambridge University Press.

Bout, R. G. (2002). Biomechanics of the avian skull. In *Vertebrate Biomechanics and Evolution* (ed. V. L. Bels, J.-P. Gasc and A. Casinos), pp. 229-242. Towbridge: Cromwell Press.

Bowman, R. I. (1961). *Morphological Differentiation and Adaptations in the Galapagos Finches*. Berkeley: University of California Publications in Zoology.

Bühler, P. (1981). The functional anatomy of the avian jaw apparatus. In *Form and Function in Birds*. Vol. 2 (ed. A. S. King and J. McLelland), pp. 439-468. London: Academic Press.

Bunday, B. D. (1984). *Basic Optimisation Methods*. London: Edward Arnold.

Díaz, M. (1990). Interspecific patterns of seed selection among granivorous passerines: effects of seed size, seed nutritive value and bird morphology. *Ibis* **132**, 467-476.

Falster, D. S., Warton, D. I. and Wright, I. J. (2003). (S)MATR: standardised major axis tests and routines. Version 1.0. http://www.bio.mq.edu.au/ecology/SMATR.

Grant, P. R. (1986). *Ecology and Evolution of Darwin's Finches*. Princeton, NJ: Princeton University Press.

Grant, B. R. and Grant, P. R. (1989). *Evolutionary Dynamics of a Natural Population: The Large Cactus Finch of the Galapagos*. Chicago: University of Chicago Press.

Grant, P. R. and Grant, B. R. (1995). Predicting microevolutionary responses to directional selection on heritable variation. *Evolution* **49**, 241-251.

Gussekloo, S. W. S., Vosselman, M. G. and Bout, R. G. (2001). Three dimensional kinematics of skeletal elements in avian prokinetic and rhynchokinetic skulls determined by roetgen stereophotogrammetry. *J. Exp. Biol.* **204**, 1735-1744.

Hammer, Ø., Harper, D. A. T. and Ryan, P. D. (2001). PAST: paleontological statistics software package for education and data analysis. Palaeontol. Electronica 4, 1-9.

Herrel, A., Podos, J., Huber, S. K. and Hendry, A. P. (2005a). Bite performance and morphology in a population of Darwin's finches: implications for the evolution of beak shape. *Funct. Ecol.* **19**, 43-48.

Herrel, A., Podos, J., Huber, S. K. and Hendry, A. P. (2005b). Evolution of bite force in Darwin's finches: a key role for head width. *J. Evol. Biol.* **18**, 669-675.

Hespenheide, H. A. (1966). The selection of seed size by finches. *Wilson Bull.* **78**, 191-197.

Hildebrand, M., Bramble, D. M., Liem, K. F. and Wake, D. B. (ed.) (1985). *Functional Vertebrate Morphology*. Cambridge, MA: Harvard University Press.

Kear, J. (1962). Food selection in finches with special reference to interspecific differences. *Proc. Zool. Soc. Lond. B* **138**, 163-204.

Merilä, J. and Björklund, M. (1999). Population divergence and morphometric integration in the greenfinch (*Carduelis chloris*) – evolution against trajectory of least resistance. *J. Evol. Biol.* **12**, 103-112.

Nuijens, F. W. and Zweers, G. A. (1997). Characters discriminating two seed husking mechanisms in finches (Fringillidae: Carduelinae) and (Passeridae: Estrildinae). *J. Morphol.* **232**, 1-33.

Nuijens, F. W., Snelderwaard, P. C. and Bout, R. G. (1997). An electromyographic technique for small animals. *J. Neurosci. Methods* **76**, 71-73.

Raikow, R. J. (1977). The origin and evolution of the Hawaiian honeycreepers (Drepanididae). *Living Bird* **15**, 95-117.

Read, J. L. (1991). Consumption of seeds by Red-browed Firetails *Neochmia temporalis* at feeders: dehusking rates and seed choice. *Corella* **15**, 19-23.

Rohlf, F. J. (1998). TpsSmall, version 1.20. Department of Ecology and Evolution, State University of New York at Stony Brook, http://life.bio.sunysb.edu/morph.

Rohlf, F. J. (2004). TpsRelw, version 1.40. Department of Ecology and Evolution, State University of New York at Stony Brook, http://life.bio.sunysb.edu/morph.

Rohlf, F. J. and Slice, D. E. (1990). Extensions of the Procrustes method for the optimal superimposition of landmarks. *Syst. Zool.* **39**, 40-59.

Schluter, D. (1982). Seed and patch selection by Galapagos ground finches: relation to foraging efficiency and food supply. *Ecology* **63**, 1106-1120.

Schluter, D. and Smith, N. M. (1986). Natural selection on beak and body size in the song sparrow. *Evolution* **40**, 221-231.

Sibley, C. G. and Monroe, B. L. (1990). *Distribution and Taxonomy of Birds of the World*. New Haven: Yale University Press.

Sibley, C. G. and Monroe, B. L. (1993). *Supplement to Distribution and Taxonomy of Birds of the World*. New Haven: Yale University Press.

Smith, T. B. (1987). Bill size polymorphism and intraspecific niche utilization in an African finch. *Nature* **329**, 717-719.

Smith, T. B. (1991). Inter- and intra-specific diet overlap during lean times between *Quelea erythrops* and bill morphs of *Pyrenestes ostrinus*. *Oikos* **60**, 76-82.
van der Meij, M. A. A. and Bout, R. G. (2000). Seed selection in the Java sparrow (*Padda oryzivora*): preference and mechanical constraint. *Can. J. Zool.* **78**, 1668-1673.
van der Meij, M. A. A. and Bout, R. G. (2004). Scaling of jaw muscle size and maximal bite force in finches. *J. Exp. Biol.* **207**, 2745-2753.
van der Meij, M. A. A. and Bout, R. G. (2006). Seed husking performance and maximal bite force in finches. *J. Exp. Biol.* **209**, 3329-3335.
van der Meij, M. A. A., Griekspoor, M. and Bout, R. G. (2004). The effect of seed hardness on husking time in finches. *Anim. Biol.* **54**, 195-205.
van der Meij, M. A. A., de Bakker, M. A. G. and Bout, R. G. (2005). A phylogeny of finches and their relatives based on nuclear and mitochondrial DNA. *Mol. Phylogenet. Evol.* **34**, 97-105.
Warton, D. I. and Weber, N. C. (2002). Common slope tests for bivariate errors-in-variables models. *Biom. J.* **44**, 161-174.
Willson, M. F. (1971). Seed selection in some North American finches. *Condor* **73**, 415-429.
Ziswiler, V. (1965). Zur kenntnis des Samenöffnens und der Struktur des hörnernen Gaumens bei körnerfressenden Oscines. *J. Ornithol.* **106**, 1-47.
Zusi, R. L. (1984). A functional and evolutionary analysis of rhynchokinesis in birds. *Smiths. Contrib. Zool.* **395**, 1-37.